Atmos. Chem. Phys. Discuss., 13, 1673–1716, 2013
www.atmos-chem-phys-discuss.net/13/1673/2013/
doi:10.5194/acpd-13-1673-2013


Atmospheric Chemistry and Physics Discussions



# Megacity impacts on regional ozone formation: observations and WRF-Chem modeling for the MIRAGE-Shanghai field campaign

**X. Tie[3,1], F. Geng[2], A. Guenther[1], J. Cao[3], J. Greenberg[1], R. Zhang[5], E. Apel[1], G. Li[3,4], A. Weinheimer[1], J. Chen[6], and C. Cai[7]**

[1]National Center for Atmospheric Research, Boulder, CO, USA
[2]Shanghai Meteorological Bureau, Shanghai, China
[3]Key Laboratory of Aerosol, SKLLQG, Institute of Earth Environment, Chinese Academy of Sciences, Xi'an, China
[4]Molina Center for Energy and the Environment, La Jolla, CA, USA
[5]Department of Atmospheric Sciences, Texas A&M, Texas 77843-3150, USA
[6]Fudan University, Shanghai, China
[7]North Carolina State University, Raleigh, North Carolina, USA







Received: 7 December 2012 – Accepted: 24 December 2012 – Published: 15 January 2013

Correspondence to: X. Tie (xxtie@ucar.edu), A. Guenther (guenther@ucar.edu)

Published by Copernicus Publications on behalf of the European Geosciences Union.





ACPD
13, 1673–1716, 2013



## Abstract

The MIRAGE-Shanghai experiment was designed to characterize the factors controlling regional air pollution near a Chinese Megacity (Shanghai) and was conducted during September 2009. This paper provides an overview of the measurements conducted for this study. In addition to the measurements, a regional chemical/dynamical model (version 3 of Weather Research and Forecasting Chemical model – WRF-Chemv3) is applied for this study. The model results are intensively compared with the measurements to evaluate the model capability for calculating air pollutants in the Shanghai region, especially the chemical species related to ozone formation. The results show that the model is able to calculate the general distributions (the level and the variability) of air pollutants in the Shanghai region, and the difference between the model calculation and the measurement are mostly smaller than 30 %, except the calculations of HONO at PD (Pudong) and CO at DT (Dongtan).

The main scientific focus is the study of ozone chemical formation not only in the urban area, but also on a regional scale of the surrounding area of Shanghai. The results show that during the experiment period, the ozone photochemical formation was strongly under the VOC-limited condition in the urban area of Shanghai. Moreover, the VOC-limited condition occurred not only in the city, but also in the larger regional area. There was a continuous enhancement of ozone concentrations in the downwind of the megacity of Shanghai, resulting in a significant enhancement of ozone concentrations in a very large regional area in the surrounding region of Shanghai. The sensitivity study of the model suggests that there is a threshold value for switching from VOC-limited condition to $NO_x$-limited condition. The threshold value is strongly dependent on the emission ratio of $NO_x$/VOCs. When the ratio is about 0.4, the Shanghai region is under a strong VOC-limited condition over the regional scale. In contrast, when the ratio is reduced to about 0.1, the Shanghai region is under a strong $NO_x$-limited condition. The estimated threshold value (on the regional scale) for switching from VOC-limited to $NO_x$-limited condition ranges from 0.1 to 0.2. This result has important implications





ACPD

13, 1673–1716, 2013



for ozone production in this region and will facilitate the development of effective $O_3$ control strategies in the Shanghai region.

## 1 Introduction

The Yangtze River Delta (YRD) located in the eastern China coast is the largest economic region in China, and Shanghai is the largest city in the region. During the past two decades, Shanghai has undergone a rapid increase in economic development. For example, the Gross Domestic Production (GDP) is over 1.49 trillion RMB, accounting for about 21 % of the total GDP in the YRD region. The number of automobiles increased from 0.47 to 2.61 million (SMSB, 2008). Accompanying the rapid economic development, the air quality has deteriorated in recent years, leading to a significant increase in the concentrations of air pollutants such as $NO_x$ and $O_3$ in Shanghai (Geng et al., 2007, 2008). Thus, a better understanding of the characteristics of precursors of $O_3$ becomes an important issue for studying ozone formation and for developing effective $O_3$ control strategies in Shanghai.

Several studies regarding the air pollution in the Shanghai region has been described (Geng et al., 2007, 2011; Tang et al., 2008; Tie et al., 2009a; Cai et al., 2010). Geng et al. (2007) suggested that $O_3$ chemical production is limited by the concentrations of VOCs in the city of Shanghai. Among the different VOC species, aromatics and alkenes play important roles for the formation of ozone. Tang et al. (2008) studied the "weekend" effect. Their study suggested that the reduction of $NO_x$ during weekend produces an increase in ozone concentrations. Tie et al. (2009) used a regional chemical/transport model (WRF-Chem) to study the variability of air pollutants in the Shanghai region, and found that meteorological conditions play important roles in controlling the variability of air pollutants in the Shanghai region. Cai et al. (2010) used a receptor model (PCA/APCS; Principal Component Analysis/Absolute Principal Component Scores) to identify the individual contributions of different VOC sources to VOC concentrations. Their result suggested that liquefied petroleum, gasoline, and solvent





ACPD
13, 1673–1716, 2013



usages had important contributions to the VOC concentrations in the Shanghai region. Geng et al. (2011) studied the effect of major forests in the south of Shanghai on ozone formation. Their result suggested that there is a large amount of isoprene which emitted from forests. As a result, the carbonyls which are formed from the process of oxidation of isoprene can be transported to the Shanghai region, and the further oxidation of the carbonyls leads to the chemical formation of ozone in Shanghai, enhancing the ozone concentration by about 20 %. These previous studies provide very useful information regarding the air pollution situations, especially ozone chemical formation in the Shanghai region. However, there is a lack of a comprehensive study, in which more chemical species are integrated together in order to get more comprehensive insights of the physical and chemical processes of the air pollutants in region. In addition, the ozone formation on a regional scale needs to be studied. Several studies (Apel et al., 2010; Tie et al., 2009b) suggested that ozone tends to be continuously produced in the city plumes in the downwind region of Mexico City. Zaveri et al. (2003) found, in the 1999 Southern Oxidant Study field campaign in Nashville, Tennessee, that the downwind $O_3$ concentrations in the Nashville plume are more sensitive to $NO_x$ emissions than anthropogenic VOC emissions. In contrast, the study of Kleinman et al. (2003) suggested that $O_3$ production is VOC limited in the high-$NO_x$ portions of the Philadelphia urban plume. Thielmann et al. (2002) suggested that at the rural area of Milan, Italy, ozone production per $NO_x$ consumed is less efficient when the advected air masses originated from Milan. However, there is a lack of studies for the ozone formation on a regional scale of the area surrounding Shanghai, which will be the scientific focus in this study.

The data used in this study is from a field experiment conducted in September 2009. The field experiment called MIRAGE-Shanghai (Megacities Impact on Regional and Global Environment – Shanghai case study) was jointly organized by the Shanghai Meteorological Bureau (SMB) and the Atmospheric Chemistry Division (ACD) of the National Center for Atmospheric Research (NCAR), with several university and research institute participant. The goal of MIRAGE-Shanghai was to characterize the





ACPD
13, 1673–1716, 2013



chemical/physical transformations associated with regional air quality. The campaign integrated observations from 7 ground stations, with 3 enhanced ground stations in different parts of the center of city as well as the rural area of the Shanghai region.

Another important goal of the experiment is to compare the observational results with model calculations. The regional chemical/dynamical model used in this study is the state of the art model, WRF-Chem. We describe an evaluation of the model performance using measurements from the field experiment. The model is then used to study the characteristics of air pollutants in the urban area and regional exports of air pollution from the urban center to the regional scale to study regional ozone formation in Shanghai and the surrounding area.

The paper is organized as follows: In Sect. 2, we will describe the field experiment as well as the regional chemical/dynamical model (WRF-Chem). In Sect. 3, the simulated chemical species will be compared to the field measurement, so as to evaluate the performance of the model. Section 4 presents model-based estimates of $O_3$ evolution in the city plumes and the regional ozone production in the surrounding area of Shanghai.

## 2 Experiment and chemical model

### 2.1 The measurement information

A comprehensive field experiment (MIRAGE-Shanghai; Megacities Impact on Regional and Global Environment at Shanghai) was conducted from 1 September to 21 September 2009. Participants in the experiment included Shanghai Meteorological Bureau (SMB), National Center for Atmospheric Research (NCAR), Fudan University, Texas A&M university, Peking University, the Institute of Chinese Meteorological Science, and the Institute of Earth and Environment (IEE) of Chinese Academy of Science (CAS). In addition to the intensive measurements of the experiment, routine measurements of air pollutants and meteorological parameters in Shanghai were conducted since 2005 at PD and DT operated by Shanghai Meteorological Bureau (SMB). The routine measure-





ACPD
13, 1673–1716, 2013



ments include CO, NO, $NO_2$, $SO_2$, $O_3$, black carbon (BC), particulate matter ($PM_{2.5}$ and $PM_{10}$), and solar radiation. The meteorological parameters include wind speed and direction, air temperature, humidity, and air pressure. In addition to the routine measurements at the 6 stations, 3 super sites were established with additional instruments for measuring air pollutants, including $NO_y$, HONO, $HNO_3$, and a more complete suite of VOC, as well as aerosol composition and size distribution. Moreover, isoprene concentrations were measured in the major forest region located south of Shanghai. The data from 2 super sites, including a site located at the urban center of the city (PD) and a remote site located at the east edge of the city along the coast of the East Sea (DT), are analyzed. These 2 sites provide useful information for comparing the characterization of air pollutants in an urban area to the situation in a remote area. The detailed information of the measured chemical species is listed in Table 1. The instruments used in this study have been used widely in various field experiments and carefully calibrated. The detailed information regarding these instruments have been described previously (Geng et al., 2007, 2008; Weinheimer et al., 1994; Guenther et al., 2006; Zheng et al., 2008; Apel et al., 2010; Molina et al., 2010). In addition to the routing measurements of $O_3$, NO, and $NO_2$ by SMB, Weinheimer et al. (1994) also used Chemiluminescence method for the measurements of $O_3$, NO, $NO_2$, and $NO_y$. The TOGA (Trace Organic Gas Analyzer) instrument continuously measured every 2.8 min 32 species including select NMHCs, halogenated compounds, and single functional non-acid OVOCs. The concentrations of $HNO_3$ and HONO were measured by ion drift-chemical ionization mass spectrometer (ID-CIMS) (Zheng et al., 2008). More detailed descriptions can be found in the above references. Figure 1 shows the measurement sites and the corresponding emission distribution of CO in the region. The detailed locations of the 2 super sites are indicated by large red circles.

### 2.2 The WRF-Chem model

The calculations presented in this study are performed using the WRF-Chem model (version-3) (Weather Research and Forecasting with Chemistry). This modeling sys-





ACPD
13, 1673–1716, 2013



tem includes two components: a dynamical module and a chemical module. WRF, used here as the dynamical module, is a mesocale numerical weather prediction system designed to serve both for operational forecasting and atmospheric research needs. The effort to develop WRF has been a partnership between the National Center for Atmospheric Research (NCAR), the National Oceanic and Atmospheric Administration (NOAA), the National Center for Environmental Prediction (NCEP), the Forecast Systems Laboratory (FSL), the Air Force Weather Agency (AFWA), the Naval Research Laboratory, the University of Oklahoma, and the Federal Aviation Administration (FAA). The model equations are solved for fully compressible and non-hydrostatic conditions. A detailed description can be found on the WRF web-site http://www.wrf-model.org/index.php. Within the WRF model, a chemical module is coupled on-line with the dynamical modules. Grell et al. (2005) gave a detailed description of the chemical component of the model. The chemical scheme of the model is represented in the model by the RADM2 (Regional Acid Deposition Model, version 2) gas phase chemical mechanism (Chang et al., 1989) which includes 158 reactions among 36 species. The model is used here with some modifications introduced by Tie et al. (2007, 2010). The model was previously applied to study the regional distributions of $O_3$ concentrations in the Shanghai region. The model result was evaluated under different weather condition. The results suggested that the model is capable for calculating the large variability of ozone concentrations and other oxidants (such as CO, $NO_x$) in the Shanghai region (Tie et al., 2009b).

For this study, the selected horizontal model resolution is 6 km in a $900 \times 900$ km domain centered around Shanghai. The anthropogenic emission inventory for $SO_2$, CO, NO, and VOCs is shown in Table 1 of Tie et al. (2009b). An example of the horizontal distribution of CO emission is shown in Fig. 1. In addition to the anthropogenic emissions, the biogenic emissions from vegetation are calculated in this model. The calculation of biogenic emission is particularly important, because this study focuses on the interaction between anthropogenic and biogenic emissions. Biogenic emissions





ACPD
13, 1673–1716, 2013



in the model are generated by a biogenic emission module (MEGAN – Model of Emissions of Gases and Aerosols from Nature) developed by Guenther et al. (2006).

## 3 Result and analysis

### 3.1 The background meteorological conditions

Figure 2 shows the rose plot of wind direction during the period from 30 August to 23 September 2009. The result shows that the prevailing winds during the experiment period were east and east-north-east winds (occurring about 62 %). As indicated in Fig. 1, the prevailing wind transported the less polluted marine air from the Pacific Ocean. However, the wind was from the north of the city for about 10 % of the time. Because there is a heavy industrial complex located in the north of the PD site, the north wind could produce high pollution events at the measurement site. The detailed effects of the wind direction are analyzed in the following sections.

Figure 3 shows the temporal variations of wind speed ($m\,s^{-1}$), wind direction (degree), and photolysis rate ($J[NO_2]$), as well as the corresponded CO, $PM_{2.5}$, and $O_3$ concentrations. It shows that the wind speed had a strong diurnal variability, with higher wind speeds during the daytime, and lower speeds during the nighttime. The range of wind speeds were from near-zero to $5\,m\,s^{-1}$, with a mean speed of about $2\,m\,s^{-1}$, indicating that the winds were not strong during the experiment period. The wind directions showed a high variability. The dominant wind direction was east wind (about 90 degree). However, during several periods, the wind directions switched from east to north winds. There were 3 major north wind periods (defined by the north winds occurring more than 2 days), occurring on 1–2, 8–10, and 12–13 September, respectively. There were also 2 minor north wind periods (defined by the north winds occurring on only one day), that happened on 6 and 19 September, respectively. The corresponded CO and $PM_{2.5}$ temporal variation showed a strong correlation with the wind direction. For example, during the major north wind period of 12–13 September, the CO and





ACPD
13, 1673–1716, 2013



$PM_{2.5}$ concentrations increased rapidly, reaching to 1.5 ppm and 130 $\mu g\,m^{-3}$ in the PD site, compared with the concentrations of 0.4–0.5 ppm and 30–50 $\mu g\,m^{-3}$ during the east wind period, suggesting that the wind direction had a significant impact on the air pollutants, especially the primary air pollutants which are directly emitted from the surface. In the following sections, we define the three major north wind periods as the "polluted period", and the east wind period as the "clean period".

Some important characterizations were also shown in the measurements in Fig. 3. First, during the "polluted period", the high aerosol loadings had an impact on the photolysis rate of J[$NO_2$]. For instance, the photolysis rate on 13 September was significantly lower than the rate on 14 September. During both days, it was clear sky condition without precipitation, suggesting that the UV radiation was reduced by heavy aerosol conditions. Second, the differences of CO, $PM_{2.5}$ and $O_3$ between the urban (PD) and remote (DT) sites were not the same. For longer lifetime species (CO), the concentrations were not very different between PD and DT during the "clean period". This result suggests that there was a background CO concentration (about 400 ppbv), which was regionally transported from surrounding areas. In contrast, for shorter lifetime species ($PM_{2.5}$), the concentrations were very different between PD and DT. The concentrations of $PM_{2.5}$ were significantly higher in the urban site (PD) than in the remote site (DT), suggesting that the local emissions of $PM_{2.5}$ dominated impacts on the $PM_{2.5}$ pollution in the urban areas of Shanghai.

### 3.2 Model evaluation

The model performance for calculating the variability of air pollutants are evaluated at 2 measurement sites (PD and DT). The differences between urban (PD) and rural areas (DT) for the characteristics of air pollutants and ozone chemical formation are analyzed from the results at the 2 sites. Figure 4 shows the measured and calculated concentrations of CO, $O_3$ and $PM_{2.5}$ at PD and DT, respectively. At the PD site, the calculated CO concentrations were generally consistent with the measured results, except that





ACPD
13, 1673–1716, 2013



the small-scale variability cannot be simulated due to the relatively coarse resolution (6 km) of the model. However, at the DT site, the calculated CO concentrations consistently underestimated the measured values during east wind periods ("clean period"). The underestimation of the CO concentrations at this remote site during east wind period suggested that the calculated long-range transport of CO was underestimated. During the north wind periods ("polluted period"), the calculated CO concentrations were elevated, indicating that the CO pollution was transported from polluted sources in Shanghai. Because there were no local CO sources at DT, the regional transport must have an important role in controlling CO concentration. In the "polluted period", the model calculation of CO was similar with the measured results, suggesting that the small-scale transport from the urban area to the remote region can be simulated by the model.

The calculated $O_3$ concentrations were very similar to the measured values at both the PD and DT sites. The calculated and measured $O_3$ concentrations showed a larger variability at PD compared with the variability at DT. Unlike the calculated CO at DT, the calculated $O_3$ concentrations were consistent with the measured value and variability. For example, the $O_3$ peak at 21 September was similar for both the measured and calculated results, indicating that the calculated photochemistry and long-range transport of $O_3$ was reasonable compared with the measured results.

The calculated $PM_{2.5}$ concentrations were generally in good agreement with the measured concentrations. The calculated temporal variability was larger, which was consistent with the measured variability. For example, during the "polluted period" (12–13 September), both the measured and calculated $PM_{2.5}$ concentrations rapidly increased. However, there was an indication that the calculated $PM_{2.5}$ concentrations were underestimated during the "clean period".

Figure 5 shows the measured and calculated temporal variations for the nitrogen family (including $NO_x$=NO + $NO_2$, $HNO_3$, HONO, and $NO_y$ (sum of the total nitrogen species)) at the urban site (PD). It shows that some of the nitrogen species, such as PAN (peroxyacetylnitrate) and MPAN (peroxymethacrylic nitrate) were not measured





ACPD
13, 1673–1716, 2013



during the experiment. However, we find that the calculated and measured ratios of $NO_x/NO_y$ were 0.92 and 0.99, respectively, indicating that the dominated nitrogen species were $NO_x$, and the missing nitrogen species had only a small contribution to the total nitrogen family during the experiment. Because $NO_x$ contained more than 90 % of total nitrogen species, the variability of $NO_x$ was similar to $NO_y$. The large variability of $NO_x$ suggested that there were large local impacts on $NO_x$ concentrations at the PD site. The calculated $HNO_3$ concentrations were consistent with measured values during the "clean period". However, during the "polluted period", the calculated $HNO_3$ concentrations overestimated the measured values. The calculated HONO concentrations were significantly underestimated compared with the measured values, indicating that some important chemical processes for the formation of HONO were not included in the current WRF-Chem model. For example, as suggested by Qin et al. (2009), the effect of relative humidity has an important impact on the formation of HONO in southern China.

Figure 6 shows several important volatile organic compounds (VOCs), including alkanes, alkenes, aromatics, and oxygenated VOCs (OVOCs). The measured values show a high variability for alkanes, with relatively high concentrations. The calculated alkane concentrations were within the range of the measured values. For example, the high episode of alkane concentrations during 12–13 September were measured and simulated. However, the high concentrations predicted by the model for 15–16 September overestimated the observed values. For the alkene concentrations, the high concentrations during the episode of 12–13 September were predicted by the model which was consistent with the measurements. However, the calculation underestimated observed values for other periods. The calculated aromatic concentrations were generally consistent with the measurements, except during some high variability events. The OVOC concentrations had a smaller variability than alkane and alkene concentrations. The calculated result was very similar to the measured values, especially during the "clean periods".





ACPD
13, 1673–1716, 2013



The overall comparison of the mean values and variation between the model calculations and the measurements are shown in Table 2 and Fig. 7. Table 2 shows that the biggest inconsistency between the model calculation and measurement is the HONO concentrations. The calculated HONO concentrations in WRF-Chem (with only gas-phase chemistry of HONO) underestimated the measured values by about 90 %, indicating that heterogeneous chemistry might play an important role in Shanghai. The high value of HONO was also measured in the PRD (Pearl River Delta) region. As shown by Qin et al. (2009), the HONO concentration measured in PRD had a maximum value of 2 ppbv, which is consistent with the measured high values of HONO in this study. The process responsible for the underestimation of HONO needs to be investigated in the future, but is out of the scope of this study. The HONO can be photolyzed to produce OH, and this process mainly occurred in the early morning (Alicke et al., 2002). Because the ozone formation is mainly happed during the daytime, the underestimation of HONO could have some (but not major) impacts on the estimation of ozone production. The other important inconsistencies between calculation and measurement include the underestimation of CO at DT. As mentioned previously, the underestimation at this remote site was mainly due to long-range transport. Other calculations indicate that the modeled mean differences were within 30 % of the measurements. For example, the calculated $O_3$ concentration differences at the PD and DT sites were within 18 and 4 % compared with the measured values. The important precursors of $O_3$ ($NO_x$ and VOCs) were within 6 and 4 %, respectively, at PD. The calculated $PM_{2.5}$ concentration was within 7 % compared with the measured mean value at the PD site. The variations of the calculated results were generally smaller than the measurements, due to the model horizontal resolution (6 km). This model evaluation suggests that the model estimates of $PM_{2.5}$ and $O_3$ and its precursors is generally consistent with measured values and the WRF-Chem model can be applied to study the processes controlling atmospheric chemistry in the Shanghai region, especially the formation of $O_3$.





ACPD
13, 1673–1716, 2013



## 4 Discussions

### 4.1 CO correlations

In an urban area, CO is mostly emitted by anthropogenic sources, such as industrial and automobile emissions. The chemical life time of CO is relatively long (a few months) (Brasseur et al., 1999). As a result, CO can be used as a regional tracer to represent a regional transport effect. In the Shanghai region, CO is not only affected by local sources in the city, but also strongly impacted by regional sources in the northwestern region (see Fig. 1). Thus, the correlation of CO with other air pollutants can provide some source information.

Figure 8 shows the CO-$PM_{2.5}$ correlation at the PD and DT sites. At the urban site (PD), the measured CO-$PM_{2.5}$ correlation showed a close correlation between CO and $PM_{2.5}$, with a $PM_{2.5}$/CO slope of 0.07 ($\mu g\,m^{-3}\,ppbv^{-1}$), indicating that the CO and $PM_{2.5}$ had a similar origin (mostly emitted from industrial and automobile sources). At the remote site (DT), CO and $PM_{2.5}$ were also closely correlated, but with a lower slope (0.026 $\mu g\,m^{-3}\,ppbv^{-1}$) than at the urban site (PD). The lower slope suggests that the resident time of $PM_{2.5}$ is shorter than CO. At both the PD and DT sites, the calculated slopes were slightly higher than the measured results, with 0.08 and 0.028 ($\mu g\,m^{-3}\,ppbv^{-1}$) at PD and DT, respectively.

Figure 9 shows the CO-$NO_x$ correlation at the PD and DT sites. At the urban site (PD), the CO-$NO_x$ correlation showed a complicated pattern with 2 distinct groups of data. For the lower concentrations of $NO_x$ (less than 20 ppbv), the CO was correlated with $NO_x$ with a $NO_x$/CO slope of 0.02, indicating a regional impact of anthropogenic emissions on $NO_x$ and CO. However, when the concentrations of $NO_x$ were very high (> 40 ppb; indicated by the dash circle), the correlation of CO-$NO_x$ was poor, suggesting that there was a strong local $NO_x$ source(s) nearby the PD site. These strong local $NO_x$ sources were also shown by the high $NO_x$ variability in Fig. 5. In contrast to the urban site (PD), at the remote site (DT), CO and $NO_x$ concentrations were closely





ACPD
13, 1673–1716, 2013



correlated. The $NO_x/CO$ slope is about 0.007 and 0.009 for the measurement and calculation, respectively. This result suggests that: (a) remote sites are under the influence of regional transport from the anthropogenic emissions of CO and $NO_x$, and (b) the lower slope (compared to the urban site) indicates that the transport of $NO_x$ to this site was smaller compared to the transport of CO due to its shorter chemical lifetime (a few hours) (Ridley et al., 1996).

The CO-VOC correlation is shown in Fig. 10, with different species of VOCs (such as CO-alkanes, CO-alkenes, CO-aromatic, and CO-OVOCs). The result shows that there was a weak correlation, for both measurements and calculations, between CO and different VOCs, with very large scatter between CO and VOC concentrations. In addition, the slopes between CO and different VOC species were different, suggesting that there was a weak similarity between the sources of CO and VOCs in the Shanghai region. As described by Cai et al. (2010) for the Shanghai region, the major alkane and alkene sources can be attributed to the petroleum industrial and vehicle source, and the major aromatic sources attributed to solvent usages and vehicle sources. As a result, the different VOC species associated with different sources had different a correlation with CO sources as indicated in Fig. 10.

### 4.2 The chemical ages

The chemical ages at the PD and DT sites are analyzed in this study. The chemical age of the city plume is defined by Kleiman (2008) and is expressed by;

$$AG = -\ln(NO_x/NO_y) \quad (1)$$

This age analysis was applied to the ozone formation in the Mexico City plume by Tie et al. (2010). Their study suggests that the age of city plumes were generally young (with AG of 1–0) near the city, and middle-aged (with AG of 1–2) or old-aged (with $AG > 2$) in the several hundred kilometers downwind of the city.

Figure 11 shows the measured (upper panel) and calculated (lower panel) chemical ages during the experiment. In the urban part of Shanghai (at PD), the measured





ACPD
13, 1673–1716, 2013



chemical ages were young, with AG being generally smaller than 1, except some occasions with AG of 1–2. The calculated AG at PD and DT shows that the values of chemical age at PD range between 0–1 (young age), which is consistent with the measured result. This result suggests that in the urban site of Shanghai, local emissions play important roles in controlling the concentrations of air pollutants. At the remote site (DT), the calculated values of chemical age were higher than the age at PD, ranging from 0–2 with frequent values of 1–2, showing that at the DT site, regional transport plays an important role in controlling the concentrations of air pollutants.

### 4.3 The ozone plumes in the region

Apel et al. (2010) and Tie et al. (2009b) showed that there was considerable ozone formation in the aged city plumes in the Mexico City region. In this study, the ozone chemical production in the aged city plumes is studied in the Shanghai region. As we mentioned before, the PD site was in the young aged plume. In order to study the ozone production in the old-age city plumes in Shanghai, the WRF-Chem model, evaluated in the Sect. 3, was applied.

Figure 12 illustrates the city plumes in 2 different cases. The first case (case-1; the upper panels) shows the calculated CO and $O_3$ plumes in the Shanghai region on 4 September, when the city pollution was defined as "clean period", with a typical east wind condition. The second case (case-2; the lower panels) shows the calculated CO and $O_3$ plumes in the Shanghai region on 12 September, when the city pollution was defined as "polluted period", with a typical north wind condition. In both cases, the long-lived CO plumes are used to trace the city plumes. As shown in Fig. 12, during the case-1, the CO concentrations have a maximum in the city, and were transported westerly to the downwind area. In contrast, the $O_3$ concentrations had a minimum in the city, and were enhanced in the downwind areas of Shanghai. During the case-2, the CO concentrations had a maximum in the city, and were transported southerly to the downwind areas of Shanghai. As the same, with the case-1, the $O_3$ concentrations had a minimum in the city, and were enhanced in the downwind areas. The evolution





ACPD
13, 1673–1716, 2013



of the CO and $O_3$ plumes along the downwind areas was clearly shown in Fig. 13. For example, in the case-1, the maximum of CO occurred at 50 km within the city, and was dispersed at 150 km from the downwind of the city. However, the $O_3$ concentrations had a minimum within 20 km of the city, and enhanced at 100–150 km downwind of the city. In the case-2, the maximum of CO occurred at 80 km within the city, and dispersed at 200 km downwind of the city. In contrast, the $O_3$ concentrations had a minimum within 20 km of the city, and enhanced at 100–300 km downwind of the city. In addition, the enhancement in the ozone was much higher in the downwind areas in case-2 than case-1, which will be investigated in the following sections.

### 4.4 Ozone formation in the city plumes

In order to analyze the ozone formation in the city plumes, the sensitivity of $O_3$ photochemical production to its main precursors (VOC and $NO_x$) in the Shanghai region is analyzed. Several previous studies (Geng et al., 2007; Ran et al., 2009; Tie et al., 2009a) suggested that the ozone formation in the city of Shanghai is limited by the concentrations of VOCs (VOC-limited). These studies also suggest that the ozone concentrations were significantly depressed by $NO_x$ concentrations in the city, indicating that the ozone formation in the urban areas of the city was VOC-limited. This VOC-limited case leads to the ozone minimum in Shanghai as shown in Fig. 12. In this study, the scientific focus is not only ozone formation in urban Shanghai, but also ozone formation on a regional scale, such as the rural and surrounding areas of Shanghai.

Figure 14 shows the ratios of $CH_2O/NO_y$ in the Shanghai region. According to the study by Sillman (1995), this ratio can be used to identify whether the ozone formation is under the VOC-limited or $NO_x$-limited conditions. For example, when the ratio of $CH_2O/NO_y$ is smaller than 0.28, the ozone formation is under the VOC-limited condition, while a ratio of $CH_2O/NO_y$ larger than 0.28 indicates ozone formation that is under the $NO_x$-limited condition. For the case-1, in the western part of Shanghai, there was a large area with a ratio smaller than 0.28, indicating that the ozone formation was in the VOC-limited region. Along the downwind city plume, the initial ozone formation





ACPD
13, 1673–1716, 2013



was strongly under the VOC-limited region (in the urban area of Shanghai). As a result, the ozone concentrations were depressed by high $NO_x$ concentrations nearby the city, leading to a minimum of ozone in the urban area.

The lower panel of Fig. 14 shows that during the case-2, the ozone formation was under the VOC-limited regime along the city plume pathway. This result suggests that ozone can be continuously produced along the pathway when additional VOCs were emitted in the city plume. According to the study by Geng et al. (2011), there is a large area of forest south of Shanghai. The biogenic emission of isoprene from the forest leads to very high isoprene concentrations in this region. According to their study, isoprene concentrations of 1–6 ppbv were measured in the forest area. These high isoprene concentrations produced important ozone production on a regional scale.

Model sensitivity runs were performed to test the hypothesis that ozone production was continuously increased by enhancement of VOCs along the city plume in the case-2, including (a) Run-0 (base run), (b) Run-1 (the emission of $NO_x$ is doubled), and (c) Run-2 (the emission of VOCs is doubled). Figure 15 shows the cross-sections (latitude-height) along the city plumes on 12 September (as indicated in Fig. 12) of the 3 model studies. The results show that in Run-0, there was an ozone minimum in the city, and ozone concentrations were enhanced downwind of the city. The result of Run-1 shows that the ozone concentrations were significantly reduced by the higher $NO_x$ concentrations compared with Run-0, indicating that in the VOC-limited regions (in the city and the surrounding areas of Shanghai), high $NO_x$ concentrations play an important role by depressing ozone concentrations. In contrast, by increasing VOC emissions, the ozone concentrations were significantly enhanced in the city plume. For example, in the 150 km downwind, the ozone concentrations were 100, 40, and 140 ppbv, for Run-0, Run-1, and Run-2, respectively. This result shows that ozone concentrations were increased by the emissions of VOCs in the city plume, which was under the VOC-limited condition.





ACPD
13, 1673–1716, 2013



### 4.5 Impact of $NO_x$/VOCs emission ratio on ozone formation

The above sensitivity study suggests that the change from VOC-limited to $NO_x$-limited conditions in Shanghai is strongly related to the ratio of $NO_x$ and VOC concentrations in the region, suggesting that changes in the emission ratio of $NO_x$/VOCs can significantly affect the ozone formation on a regional scale. Thus, it is important to find a threshold value of emission ratio ($NO_x$/VOC) in the Shanghai region, under which the VOC-limited condition is switched to a $NO_x$-limited condition. According to the studies by Apel et al. (2010), the concentration ratio of $NO_x$/VOC in Mexico City in 2006 was about 0.36, with an emission ratio of 0.1 (Tie et al., 2010). In contrast, the $NO_x$/VOCs ratio in Shanghai was about 0.9, with an emission ratio of 0.4 in this study, which was much higher than Mexico City. In Mexico City, the major fuel used for industrial and human activities is oil/gas, while in Shanghai the major fuel is the coal. The difference of the major fuel usages in the two megacities causes a very different $NO_x$/VOCs emission ratio. Under the lower emission ratio (e.g. in Mexico City), the ozone formation was VOC-limited only in the center of the city, while in the rural and surrounding areas of Mexico City, the ozone formation was under the $NO_x$-limited condition. However, in the Shanghai region, because the ratio of $NO_x$/VOCs was very high, it resulted in a very strong VOC-limited condition on a regional scale. As a result, the ozone concentration was continuously increased in the city plumes. According to the study by Tie et al. (2009b) and Geng et al. (2011), the ozone enhancement downwind of the city was mainly attributed to 3 factors: including (a) the oxidation of OVOCs in the plumes, (b) the oxidation of CO in the plumes, and (c) the biogenic emission of isoprene. These important factors for affecting the ozone formation in the Shanghai region are shown in Fig. 16. The figure shows that the OH reactivity for CO had high values in a wide region surrounding the city, especially in the city plume. The OH reactivity of OVOCs had the most important impact on the ozone formation in the city plume downwind of the city. This result is consistent with the study by Tie et al. (2010) for the Mexico City case. The OH reactivity due to the biogenic emission of VOCs (isoprene) had an important effect





ACPD
13, 1673–1716, 2013



on ozone formation in the major forest located south of Shanghai, which is consistent with the result of Geng et al. (2011). The above study suggests that understanding the regional ozone formation (either under VOC or $NO_x$ limited condition) has very important implications for ozone pollution control not only in the urban area of large cities, but also on a regional scale for the areas surrounding large cities.

In order to quantify the effect of the emission ratio of $NO_x$/VOCs on the ozone formation condition on a regional scale, 4 different model runs are performed in this study, including (a) the emission ratio of 0.4 (Run-R1), (b) the emission ratio of 0.8 (Run-R2), (c) the emission ratio of 0.2 (Run-R3), and (d) the emission ratio of 0.1 (Run-R4). The result with these 4 model runs is shown in Fig. 17. The figure shows that with the ratio of 0.4 (base run in the model), the city of Shanghai was under a very strong VOC-limited condition. In addition the urban area of the city, a large regional area, especially in the downwind city plume, the ozone formation was also under the VOC-limited condition. With the enhancement of $NO_x$ emissions in the model (Run-R2 with the ratio of 0.8), most regions in the areas surrounding Shanghai, except the ocean area, was under the VOC-limited condition, under which the enhancement of $NO_x$ strongly depressed the ozone formation in the region. In contrast, by reducing $NO_x$ emissions or increasing VOC emission (Run-R3 with the ratio of 0.2), the VOC-limited areas were significantly reduced, and the $NO_x$-limited condition dominated the region. By further reducing $NO_x$ emissions or increasing VOC emission (Run-R4 with the ratio of 0.1), the VOC-limited condition was limited to the center of large cities, and the ozone formation was strongly controlled by the $NO_x$-limited condition in the region. The ozone formation was enhanced by the increase of $NO_x$ emission in most regions including in the city plumes. This result suggests that the emission ratio of $NO_x$/VOC is very sensitive to whether the region is under VOC or $NO_x$ limited conditions, with a threshold emission ratio between 0.1 and 0.2 on a regional scale around the Shanghai region. When the ratio is greater than 0.8, the ozone formation is not sensitive to the emission ratio. Under this high ratio condition, the entire region is under strong VOC-limited conditions for the formation of ozone.





ACPD
13, 1673–1716, 2013



## 5 Summary

The highlights of the results of this study of the Shanghai region are

1. The air pollution had very strong variability due to the influences of meteorological conditions, especially the wind direction. The air pollution was low with the east wind and much higher with the north wind.

2. The model is able to simulate most of the measured chemical species, including CO, $O_3$, $PM_{2.5}$, the nitrogen family, and most VOC species (alkanes, alkenes, aromatics, and OVOCs), with the differences between model simulated and measured values being smaller than 30 %. However, some discrepancies are also noticeable. For example, the calculated HONO significantly underestimated the measured values (90 %), with only gas-phase HONO chemistry in the model.

3. The correlation between air pollutants and CO suggests that CO and $PM_{2.5}$ had a very similar origination (emission sources) in the Shanghai region. However, the slopes between CO and specific VOC species were different, suggesting that there was a weak similarity between the sources of CO and VOCs in the Shanghai region, due to fact that different VOC species were emitted from different source originations.

4. During the experiment period, the ozone photochemical formation was strongly VOC-limited. The VOC-limited condition occurred not only in the urban area, but also in a large regional area surrounding Shanghai. In addition, the regional distribution of VOC-limited conditions changes with different meteorological conditions. The VOC-limited area was larger for north wind condition (polluted period) than east wind condition (clean period).

5. The ozone formation was enhanced in the city plumes in the downwind region because the city plumes were under VOC-limited conditions, resulting in an enhanced ozone formation in a large regional area. This study suggests that ozone





ACPD
13, 1673–1716, 2013



was continuously produced in the city plumes and could be mainly attributed to the oxidation of OVOCs in the plumes, the oxidation of CO in the plumes, and the biogenic emission of isoprene.

6. The threshold value of the emission ratio ($NO_x$/VOC), under which the ozone formation is switched from VOC-limited to $NO_x$-limited conditions, is studied in the Shanghai region. It shows that with the ratio of 0.4 (base run in the model), the city of Shanghai was under a very strong VOC-limited condition. In addition, a large region, including the urban area of the city and the downwind city plume, was under the VOC-limited condition. With the enhancement of $NO_x$ emissions in the model (Run-R2 with the ratio of 0.8) most regions in the areas surrounding Shanghai were under the VOC-limited condition. By reducing $NO_x$ emissions or increasing VOC emission (Run-R3 with the ratio of 0.2), the VOC-limited areas were significantly reduced, and the $NO_x$-limited condition dominated in the region. By further reducing $NO_x$ emissions or increasing VOC emission (Run-R4 with the ratio of 0.1), the VOC-limited condition was limited only in the urban center, and the ozone formation was strongly controlled by the $NO_x$-limited condition in the region. This result suggests that VOC or $NO_x$ limited conditions on the regional scale are very sensitive to the emission ratio of $NO_x$/VOC. The emission ratio of the threshold value for switching from the VOC-limited to $NO_x$-limited conditions ranges from 0.1 and 0.2 in the Shanghai region.

**Supplementary material related to this article is available online at: http://www.atmos-chem-phys-discuss.net/13/1673/2013/acpd-13-1673-2013-supplement.pdf.**

*Acknowledgements.* This research is partially supported by National Natural Science Foundation of China (NSFC) under Grant No. 41275168. The National Center for Atmospheric Research is sponsored by the National Science Foundation.





ACPD
13, 1673–1716, 2013



## References


Alicke, B., Platt, U., and Stutz, J.: Impact of nitrous acid photolysis on the total hydroxyl radical budget during the Limitation of Oxidant Production/Pianura Padana Produzione di Ozono study in Milan, J. Geophys. Res., 107, 8196, doi:10.1029/2000JD000075, 2002.

Apel, E. C., Emmons, L. K., Karl, T., Flocke, F., Hills, A. J., Madronich, S., Lee-Taylor, J., Fried, A., Weibring, P., Walega, J., Richter, D., Tie, X., Mauldin, L., Campos, T., Weinheimer, A., Knapp, D., Sive, B., Kleinman, L., Springston, S., Zaveri, R., Ortega, J., Voss, P., Blake, D., Baker, A., Warneke, C., Welsh-Bon, D., de Gouw, J., Zheng, J., Zhang, R., Rudolph, J., Junkermann, W., and Riemer, D. D.: Chemical evolution of volatile organic compounds in the outflow of the Mexico City Metropolitan area, Atmos. Chem. Phys., 10, 2353–2375, doi:10.5194/acp-10-2353-2010, 2010.

Brasseur, G., Orlando, J., and Tyndall, G.: Atmospheric Chemistry and Global Change, Oxford University Press, NY, USA, 1999.

Cai, C. J., Geng, F. H., Tie, X., Yu, X. Q., and An, J. L.: Characteristics and source apportionment of VOCs measured in Shanghai, China, Atmos. Environ., 44, 5005–5014, doi:10.1016/j.atmosenv.2008.05.045, 2010.

Chang, J. S., Binkowski, F. S., Seaman, N. L., McHenry, J. N., Samson, P. J., Stockwell, W. R., Walcek, C. J., Madronich, S., Middleton, P. B., Pleim, J. E., and Lansford, H. H.: The regional acid deposition model and engineering model, State-of-Science/Technology, Report 4, National Acid Precipitation Assessment Program, Washington, DC, 1989.

Geng, F. H., Zhao, C. S., Tang, X., Lu, G. L., and Tie, X.: Analysis of ozone and VOCs measured in Shanghai: a case study, Atmos. Environ., 41, 989–1001, 2007.

Geng, F. H., Tie, X., Xu, J., Zhou, G., Peng, L., Gao, W., Tang, X., and Zhao, C.: Characterization of $O_3$, $NO_x$ and VOCs measured in Shanghai, China, Atmos. Environ., 42, 6873–6883, 2008.

Geng, F., Tie, X., Guenther, A., Li, G., Cao, J., and Harley, P.: Effect of isoprene emissions from major forests on ozone formation in the city of Shanghai, China, Atmos. Chem. Phys., 11, 10449–10459, doi:10.5194/acp-11-10449-2011, 2011.

Guenther, A., Karl, T., Harley, P., Wiedinmyer, C., Palmer, P. I., and Geron, C.: Estimates of global terrestrial isoprene emissions using MEGAN (Model of Emissions of Gases and Aerosols from Nature), Atmos. Chem. Phys., 6, 3181–3210, doi:10.5194/acp-6-3181-2006, 2006.






ACPD
13, 1673–1716, 2013



Grell, G. A., Peckham, S. E., Schmitz, R., McKeen, S. A., Wilczak, J., and Eder, B.: Fully coupled "online" chemistry within the WRF model, Atmos. Environ., 39, 6957–6975, 2005.

Kleinman, L. I., Daum, P. H., Lee, Y.-N., Nunnermacker, L. J., Springston, S. R., Weinstein-Lloyd, J., Hyde, P., Doskey, P., Rudolph, J., Fast, J., and Berkowitz, C.: Photochemical age determinations in the Phoenix metropolitan area, J. Geophys. Res., 108, 4096, doi:10.1029/2002JD002621, 2003.

Molina, L. T., Madronich, S., Gaffney, J. S., Apel, E., de Foy, B., Fast, J., Ferrare, R., Herndon, S., Jimenez, J. L., Lamb, B., Osornio-Vargas, A. R., Russell, P., Schauer, J. J., Stevens, P. S., Volkamer, R., and Zavala, M.: An overview of the MILAGRO 2006 Campaign: Mexico City emissions and their transport and transformation, Atmos. Chem. Phys., 10, 8697–8760, doi:10.5194/acp-10-8697-2010, 2010.

Qin, M., Xie, P., Su, H., Gu, J., Peng, F., Li, S., Zeng, L., Liu, J., Liu, W., and Zhang, Y.: An observational study of the HONO–$NO_2$ coupling at an urban site in Guangzhou City, South China, Atmos. Eviron., doi:10.1016/j.atmosenv.2009.08.017, 2009.

Ran, L., Zhao, C. S., Geng, F. H., Tie, X., Tang, X., Peng, L., Zhou, G. Q., Yu, Q., Xu, J. M., and Guenther, A.: Ozone photochemical production in urban Shanghai, China: analysis based on ground level observations, J. Geophys. Res., 114, D15301, doi:10.1029/2008JD010752, 2009.

Ridley, B. A., Dye, J. E., Walega, J. G., Zheng, J., Grahek, F. E., and Rison, W.: On the production of active nitrogen by thunderstorms over New Mexico, J. Geophys. Res., 101, 20985–21006, 1996.

Sillman, S.: The use of $NO_y$, $H_2O_2$, and $HNO_3$ as indicators for ozone-$NO_x$-hydrocarbon sensitivity in urban locations, J. Geophys. Res., 100, 14175–14188, 1995.

Shanghai Municipal Statistics Bureau (SMSB): Shanghai Statistical Yearbook (in Chinese), China Statistical Press,43, 5731–5742, 2008.

Tang, W. Y., Zhao, C. S., Geng, F. H., and Tie, X.: Study of ozone "weekend effect" in Shanghai, Sci. China, 51, 1354–1360, 2008.

Thielmann, A., Prévôt, A. S. H., and Staehelin, J.: Sensitivity of ozone production derived from field measurements in the Italian Po basin, J. Geophys. Res., 107, 8194, doi:10.1029/2000JD000119, 2002.

Tie, X., Madronich, S., Li, G. H., Ying, Z. M., Zhang, R., Garcia, A., Lee-Taylor, J., and Liu, Y.: Characterizations of chemical oxidants in Mexico City: a regional chemical/dynamical model (WRF-Chem) study, Atmos. Environ., 41, 1989–2008, 2007.





ACPD
13, 1673–1716, 2013



Tie, X., Geng, F. H., Peng, L., Gao, W., and Zhao, C. S.: Measurement and modeling of $O_3$ variability in Shanghai, China; application of the WRF-Chem model, Atmos. Environ., 43, 4289–4302, 2009a.

Tie, X., Madronich, S., Li, G., Ying, Z., Weinheimer, A., Apel, E., and Campos, T.: Simulation of Mexico City plumes during the MIRAGE-Mex field campaign using the WRF-Chem model, Atmos. Chem. Phys., 9, 4621–4638, doi:10.5194/acp-9-4621-2009, 2009b.

Tie, X., Brasseur, G., and Ying, Z.: Impact of model resolution on chemical ozone formation in Mexico City: application of the WRF-Chem model, Atmos. Chem. Phys., 10, 8983–8995, doi:10.5194/acp-10-8983-2010, 2010.

Velasco, E., Lamb, B., Westberg, H., Allwine, E., Sosa, G., Arriaga-Colina, J. L., Jobson, B. T., Alexander, M. L., Prazeller, P., Knighton, W. B., Rogers, T. M., Grutter, M., Herndon, S. C., Kolb, C. E., Zavala, M., de Foy, B., Volkamer, R., Molina, L. T., and Molina, M. J.: Distribution, magnitudes, reactivities, ratios and diurnal patterns of volatile organic compounds in the Valley of Mexico during the MCMA 2002 & 2003 field campaigns, Atmos. Chem. Phys., 7, 329–353, doi:10.5194/acp-7-329-2007, 2007.

Weinheimer, A. J., Walega, J. G., Ridley, B. A., Gary, B. L., Blake, D. R., Blake, N. J., Rowland, F. S., Sachse, G. W., Anderson, B. E., and Collins, J. E.: Meridional distributions of $NO_x$, $NO_y$, and other species in the lower stratosphere and upper troposphere during AASE II, Geophys. Res. Lett., 21, 2583–2586, 1994.

Zaveri, R. A., Berkowitz, C. M., Kleinman, L. I., Springston, S. R., Doskey, P. V., Lonneman, W. A., and Spicer, C. W.: Ozone production efficiency and $NO_x$ depletion in an urban plume: interpretation of field observations and implications for evaluating $O_3$-$NO_x$-VOC sensitivity, J. Geophys. Res., 108, 4436, doi:10.1029/2002JD003144, 2003.

Zheng, J., Zhang, R., Fortner, E. C., Volkamer, R. M., Molina, L., Aiken, A. C., Jimenez, J. L., Gaeggeler, K., Dommen, J., Dusanter, S., Stevens, P. S., and Tie, X.: Measurements of $HNO_3$ and $N_2O_5$ using ion drift-chemical ionization mass spectrometry during the MILAGRO/MCMA-2006 campaign, Atmos. Chem. Phys., 8, 6823–6838, doi:10.5194/acp-8-6823-2008, 2008.





ACPD
13, 1673–1716, 2013



**Table 1.** List of institutions and instruments deployed at the PD and DT sites.

| |
|---|
| PD site |
| Shanghai Meteorological Bureau (SMB)<br>$O_3$, CO, NO, $NO_2$, $SO_2$,<br>BC, $PM_1$, $PM_{2.5}$, $PM_{10}$,<br>Meteorological data (MET), including winds, temperature, pressure, RH<br>$J[NO_2]$, Lidar |
| Atmospheric Chemistry Division (ACD), NCAR<br>$O_3$, NO, $NO_2$, $NO_y$<br>Light NMHCs (online)<br>NHMCs, including OVOCs (online)<br>Analysis of biogenic VOCs sampled in southern forest |
| University of Texas A&M<br>$HNO_3$, HONO |
| DT site |
| Shanghai Meteorological Bureau (SMB)<br>$O_3$, CO, NO, $NO_2$,<br>BC, $PM_1$, $PM_{2.5}$, $PM_{10}$,<br>Meteorological data (MET), including winds, temperature, pressure, RH<br>$J[NO_2]$ |
| Atmospheric Chemistry Division (ACD), NCAR<br>NHMCs (cartridges) |





ACPD
13, 1673–1716, 2013



**Table 2.** Comparison of the calculated mean values (variances) at the PD and DT sites with the measured results.

| Species | sites | Measured Mean | Measured (Vari) | Calculated Mean | Calculated (Vari) | Meas-Calcu Diff | Meas-Calcu Diff (%) |
|---|---|---|---|---|---|---|---|
| CO (ppb) | PD | 440 | (206) | 479. | (178) | −40 | −6 |
| | DT | 327 | (94) | 173 | (92) | 54. | 47 |
| $O_3$ (ppb) | PD | 35.0 | (17.7) | 41.2 | (13.8) | −6.2 | −17.9 |
| | DT | 48.9 | (10.7) | 50.9 | (11.3) | −2.0 | −4.1 |
| $PM_{2.5}$ ($\mu g\,m^{-3}$) | PD | 36.4 | (16.7) | 33.9 | (21.8) | 2.5 | 6.8 |
| | DT | 6.0 | (4.1) | | | | |
| $NO_x$ (ppb) | PD | 22.5 | (12.4) | 21.2 | (16.5) | 1.3 | 5.8 |
| | DT | 2.0 | (1.5) | | | | |
| $NO_y$ (ppb) | PD | 22.5 | (13.3) | 23.8 | (14.3) | −1.3 | −5.8 |
| $HNO_3$ (ppb) | PD | 1.08 | (0.61) | 1.42 | (1.15) | −0.3 | −31.4 |
| HONO (ppb) | PD | 0.58 | (0.31) | 0.06 | (0.03) | 0.5 | 89.6 |
| Alkane (ppb) | PD | 12.41 | (5.36) | 10.96 | (12.24) | 1.4 | 11.6 |
| Alkene (ppb) | PD | 4.27 | (9.50) | 5.16 | (4.93) | −0.8 | −20.8 |
| Aromatic (ppb) | PD | 2.71 | (3.10) | 1.91 | (2.58) | 0.8 | 29.5 |
| OVOCs (ppb) | PD | 5.13 | (2.60) | 6.03 | (4.80) | −9.0 | 17.5 |
| VOC_sum (ppb) | PD | 24.53 | | 24.06 | | 0.4 | 1.8 |





ACPD
13, 1673–1716, 2013



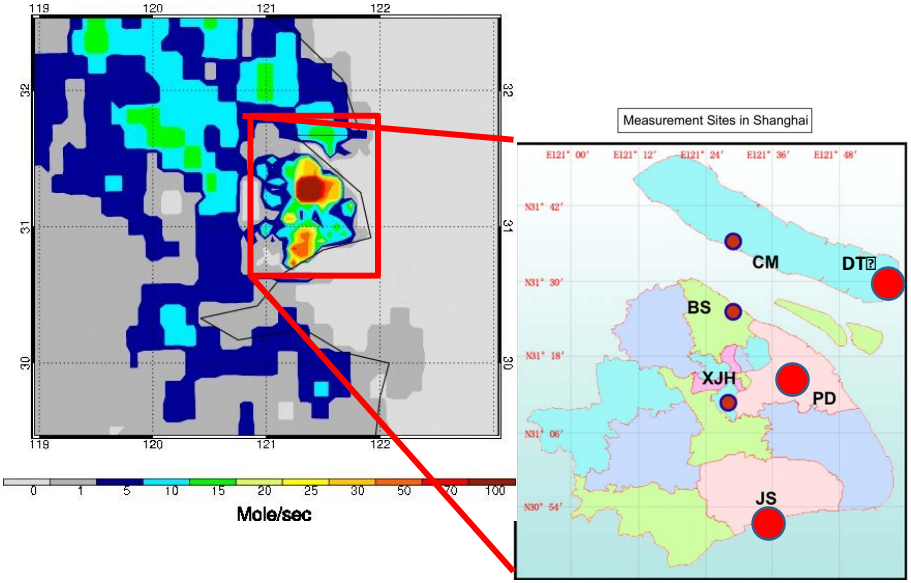


**Fig. 1.** The measurement sites (right panel) and the corresponding emission distribution of CO (left panel) in the Shanghai region. The large red points show the 2 super sites during the field experiment. The white points indicate the routine measurement sites operated by SMB.





ACPD
13, 1673–1716, 2013



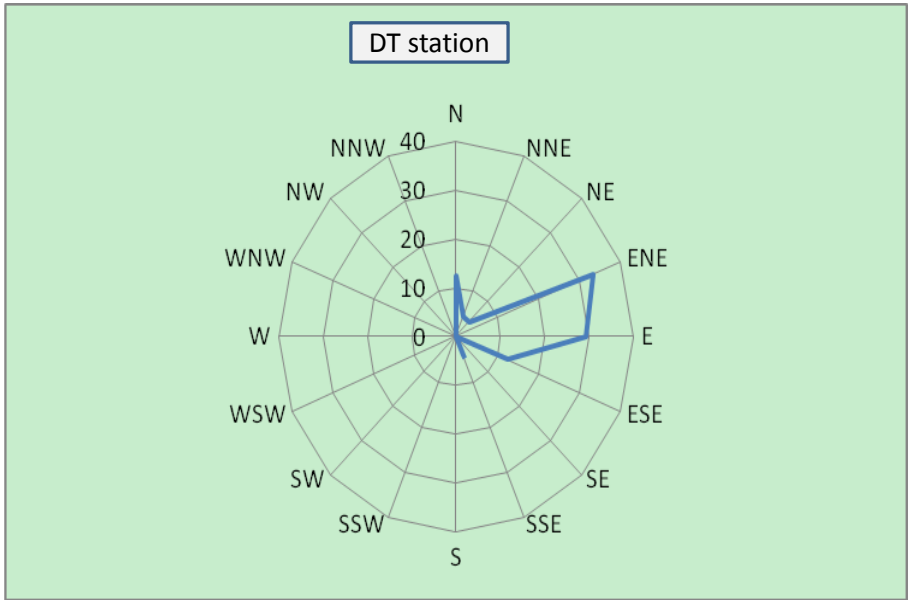


**Fig. 2.** The rose plot of wind direction at DT station during 30 August to 23 September 2009. The main wind direction is E and ENE (62 %). There is also N wind (10 %), which can transport pollutants to the city center of Shanghai.





ACPD
13, 1673–1716, 2013



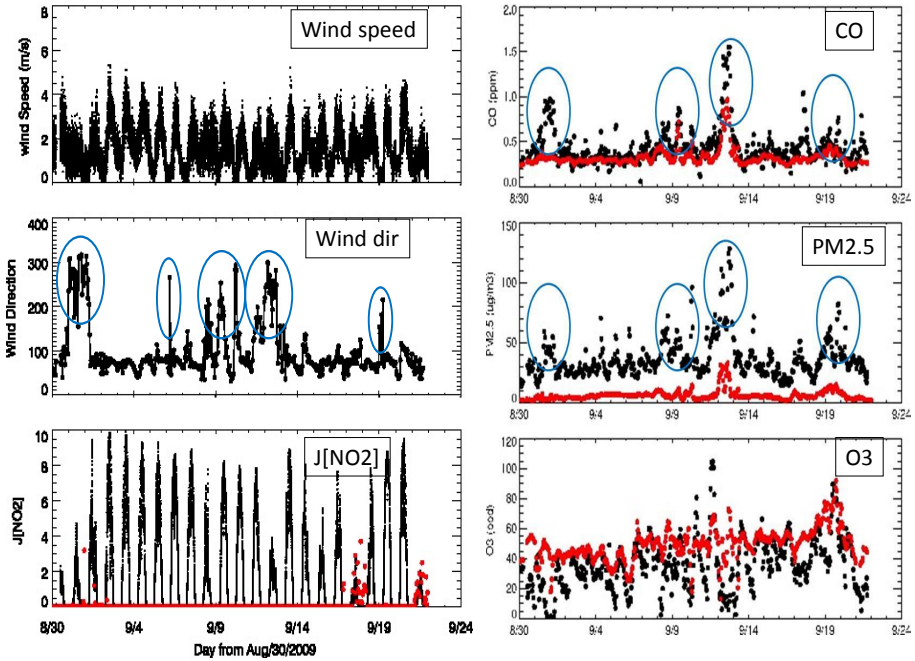


**Fig. 3.** Measured temporal variations of wind speed ($m s^{-1}$), wind direction (degree), and photolysis rate ($J[NO_2]$) (left panels) at DT site (the red dots in this panel indicates the amount of precipitation). The right panels show the corresponding measured temporal variations CO, $PM_{2.5}$, and $O_3$ concentrations at PD (black dots) and at DT (red dots).





ACPD
13, 1673–1716, 2013



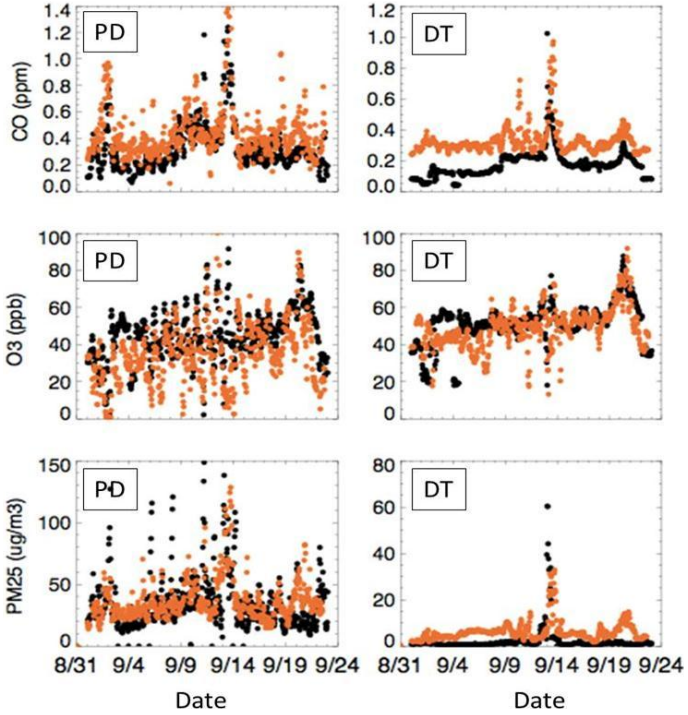


**Fig. 4.** The measured and calculated CO and $O_3$ variability at PD (left panels) and DT sites (right panels). The measured results are represented by the orange dots and calculated results by the black dots, respectively.





ACPD
13, 1673–1716, 2013



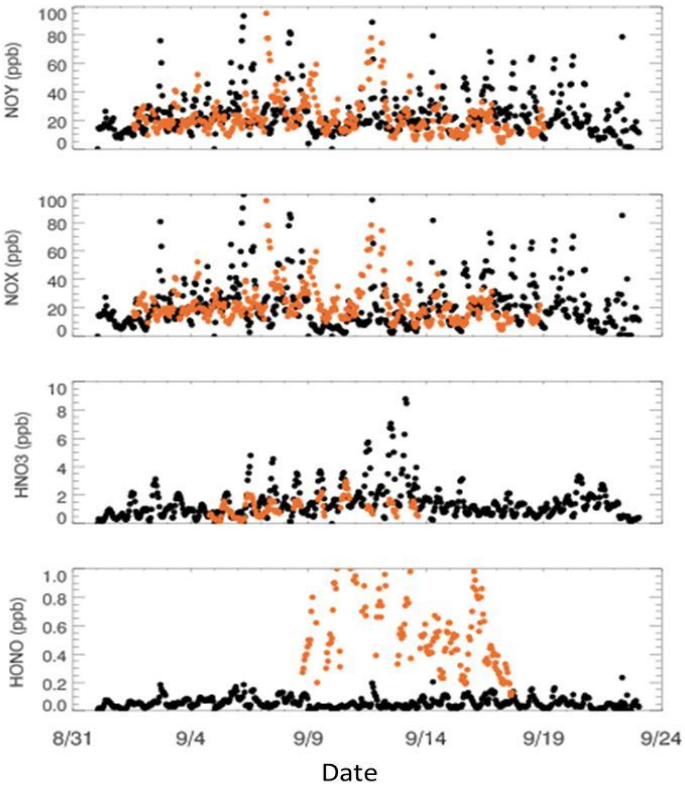


**Fig. 5.** The measured (orange dots) and calculated (black dots) temporal variability of $NO_y$, $NO_x$, $HNO_3$, and HONO concentrations at PD station.





ACPD
13, 1673–1716, 2013





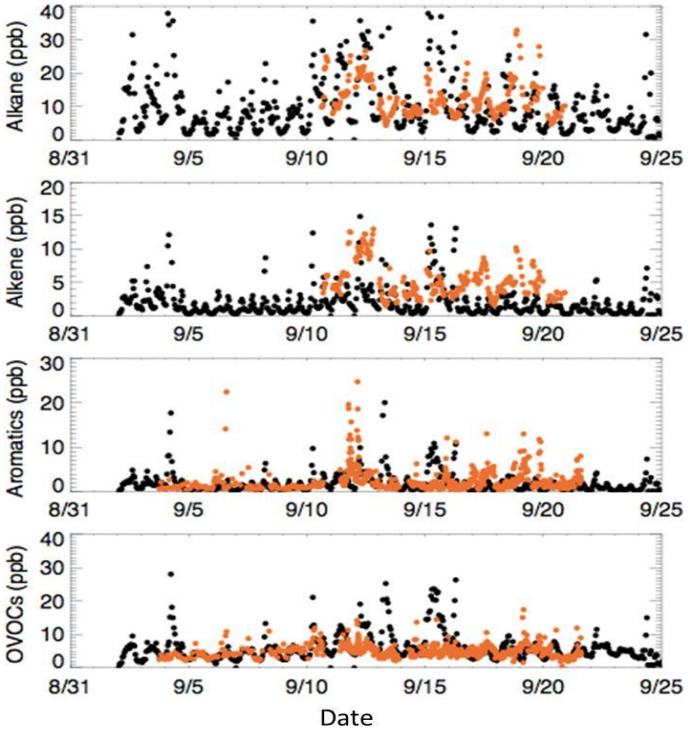


**Fig. 6.** The measured (orange dots) and calculated (black dots) temporal variability of VOC concentrations as alkanes, alkenes, aromatics, and OVOCs at the PD site.





ACPD
13, 1673–1716, 2013



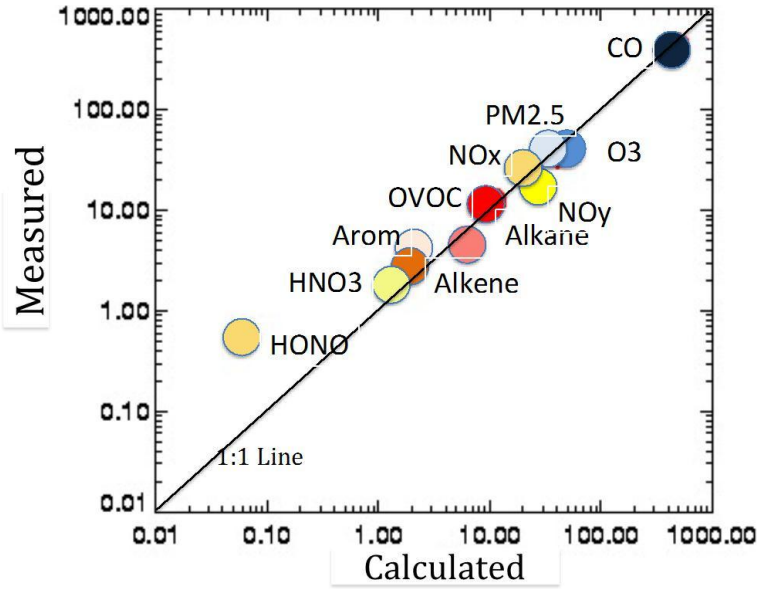


**Fig. 7.** Comparisons of the mean values of measured (y-coordinate) and calculated (y-coordinate) air pollutants (CO, $O_3$, $PM_{2.5}$, etc.) at the PD site.





ACPD
13, 1673–1716, 2013



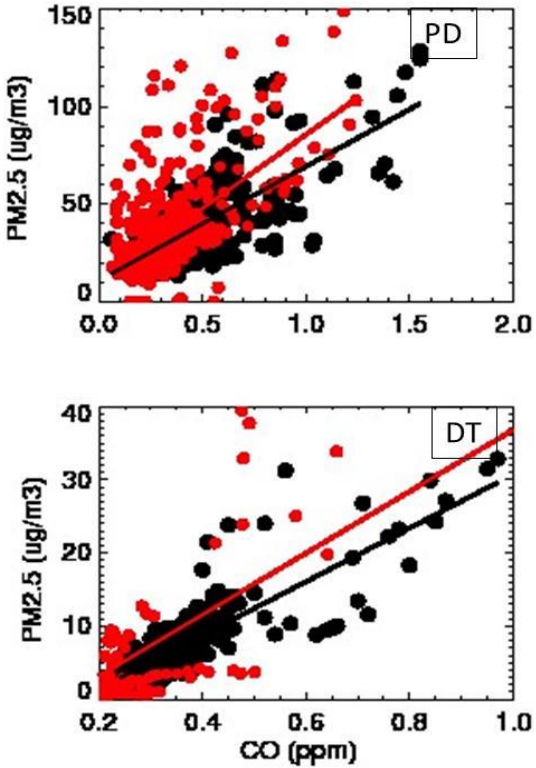


**Fig. 8.** The measured (black dots) and calculated (red dots) correlation of CO-$PM_{2.5}$ at the PD (upper panel) and DT (lower panel) sites.





ACPD
13, 1673–1716, 2013



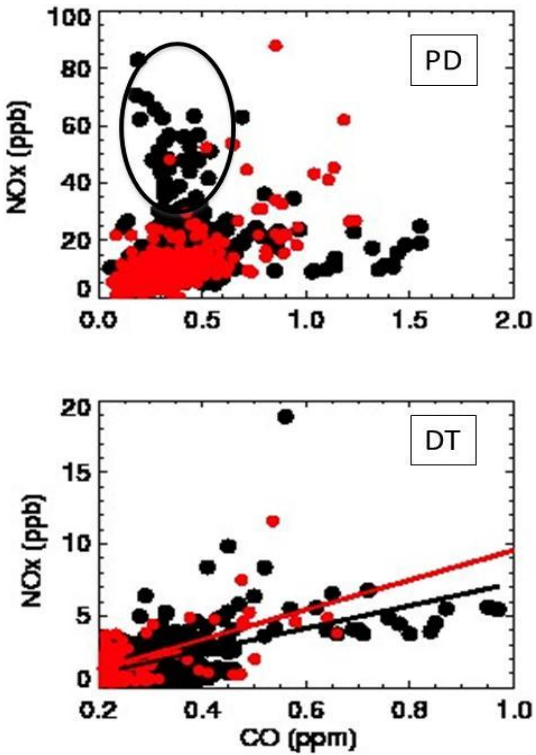


**Fig. 9.** Same as Fig. 8, except for the correlation of CO-$NO_x$. The dashed circle in the upper panel indicates the local $NO_x$ pollution at the urban area of Shanghai (PD).





ACPD
13, 1673–1716, 2013



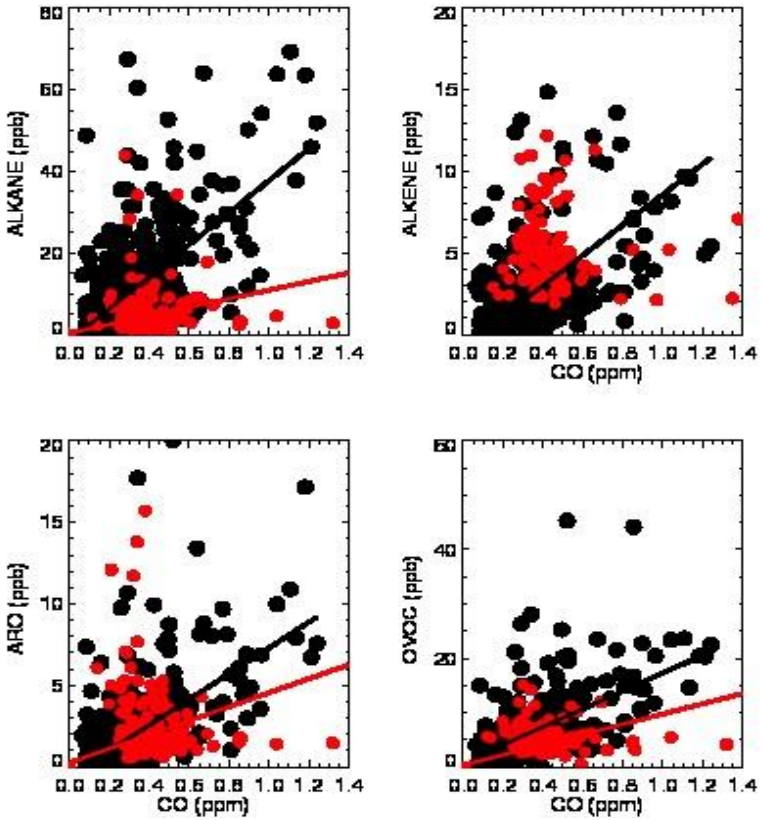


**Fig. 10.** Same as Fig. 8, except for the correlation of CO-VOCs.





ACPD
13, 1673–1716, 2013



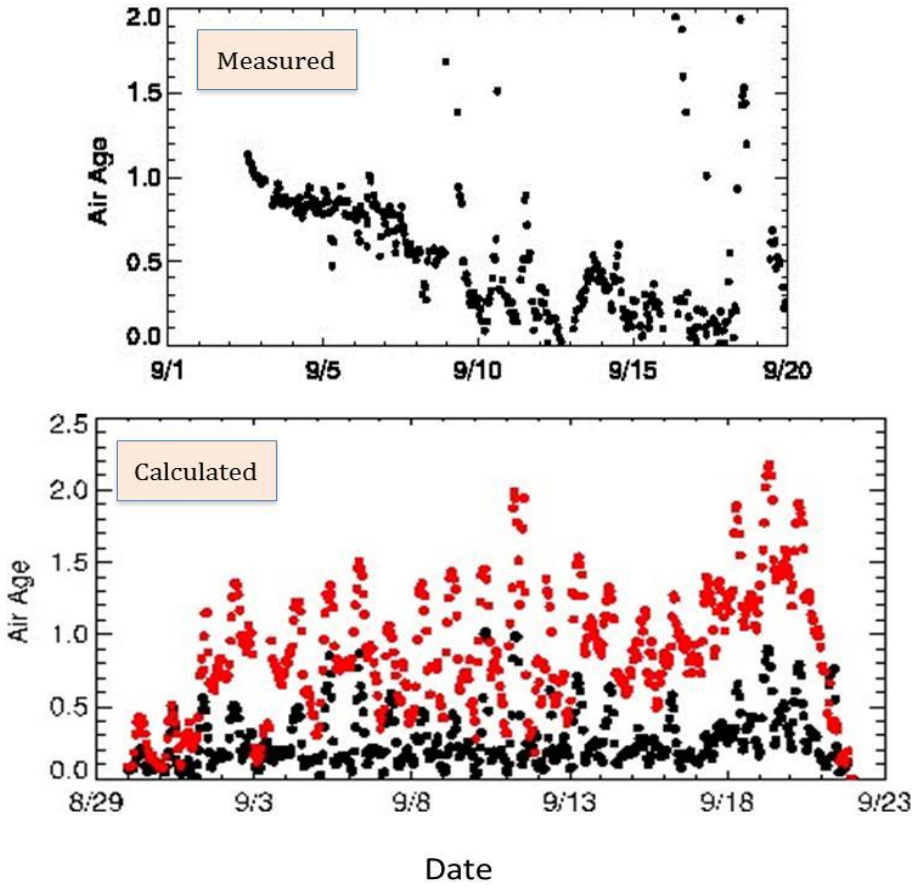


**Fig. 11.** The measured (upper panel) and calculated (lower panel) chemical ages during the experiment. In the calculated ages, the black and red dots represent the ages at the PD and DT sites, respectively.





ACPD
13, 1673–1716, 2013



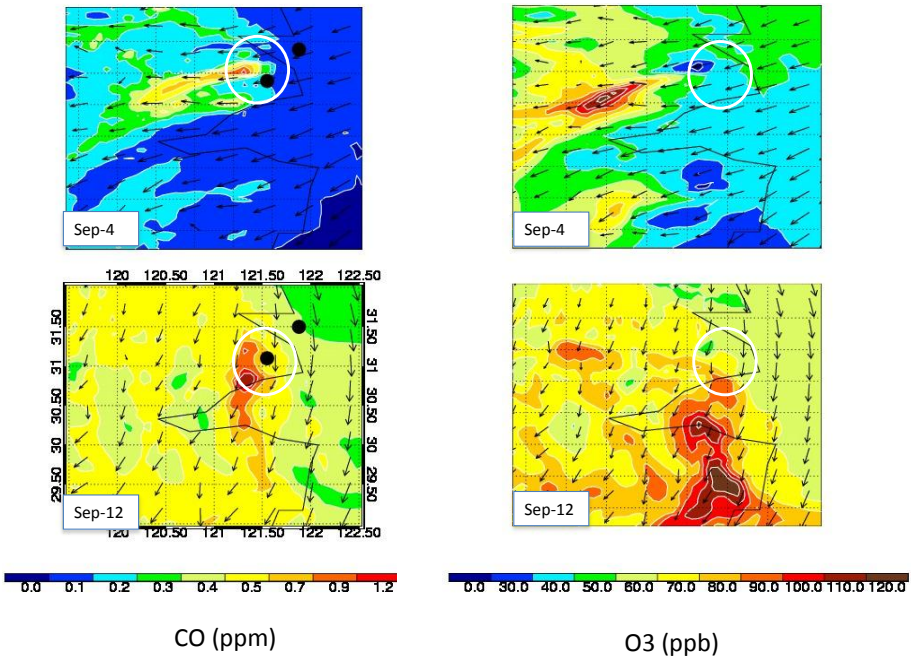


**Fig. 12.** The calculated horizontal distribution of CO in different meteorological conditions. The upper panel shows a typical eastern wind condition in 4 September, resulting in a lower CO concentrations in the Shanghai region. The lower panel shows a typical northern wind condition, producing higher CO concentration in the Shanghai region.





ACPD
13, 1673–1716, 2013



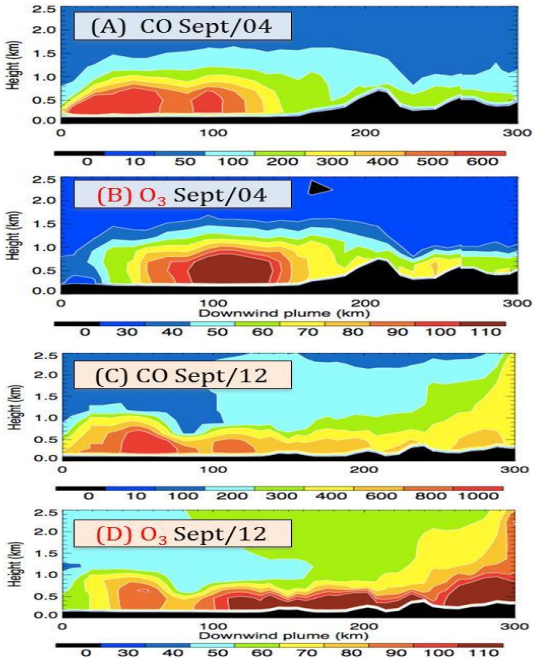


**Fig. 13.** The calculated cross-section (altitude-downwind distances) of the city plumes of CO and $O_3$ on 4 September (clean period) and 12 September (polluted period), respectively.





ACPD
13, 1673–1716, 2013



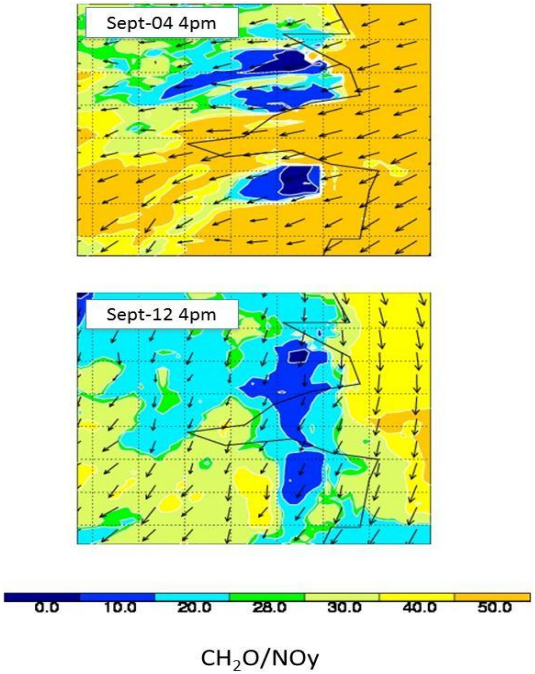


**Fig. 14.** The calculated ratio of $CH_2O/NO_y$ on 4 September (clean period) and 12 September (polluted period), respectively. When the ratio is less than 0.28 (as indicated by the blue area), the area is under the VOC-limited condition for ozone formation, while a higher ratio indicates that the area is under the $NO_x$-limited condition.





ACPD
13, 1673–1716, 2013



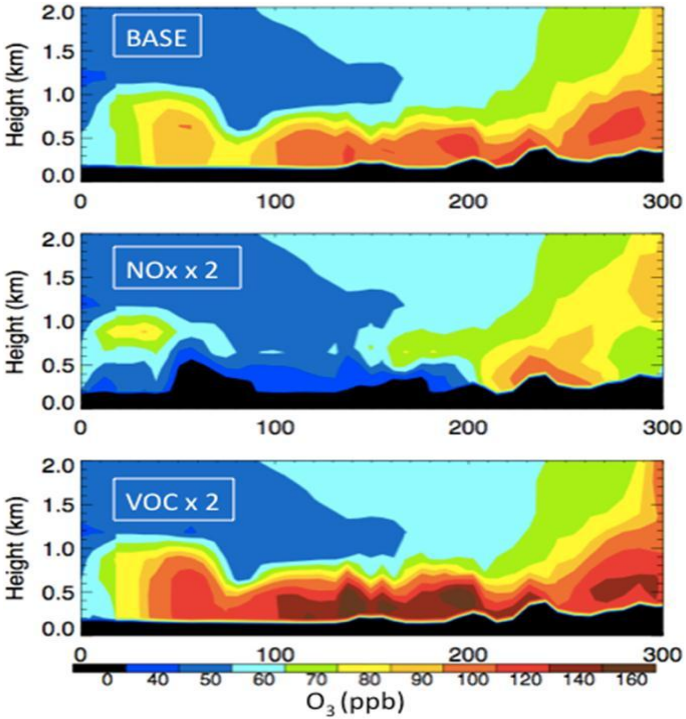


**Fig. 15.** The calculated cross-section (altitude-downwind distances) of the city plumes of $O_3$ on 12 September, due to different emissions, such as the base model run (upper panel), doubled $NO_x$ emissions (midel panel), and doubled VOC emissions (lower panel).





ACPD
13, 1673–1716, 2013



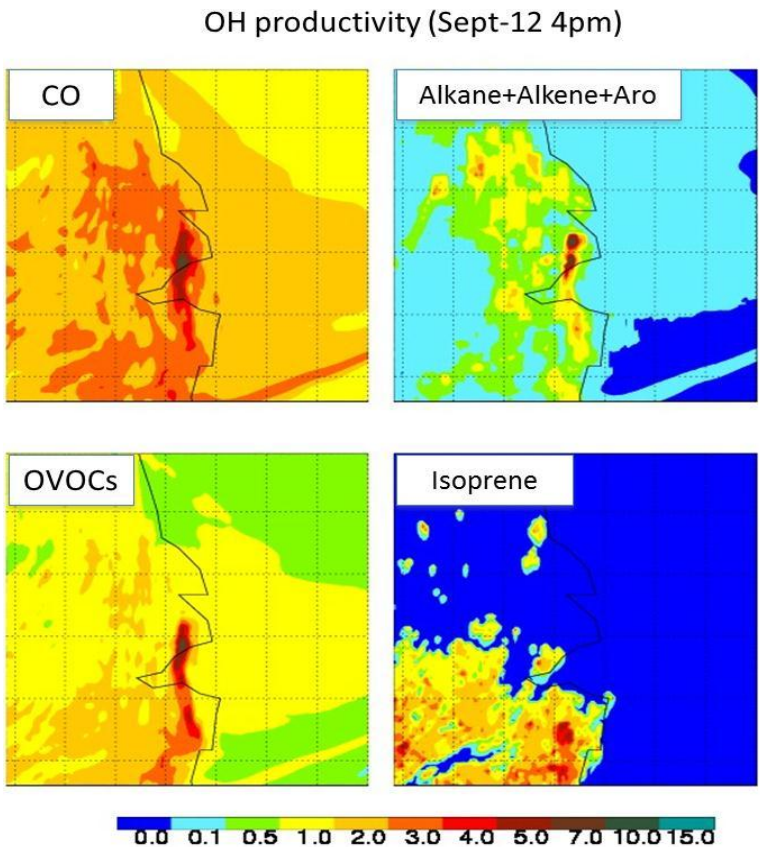


**Fig. 16.** The calculated OH reactivity for different species in the Shanghai region, including CO, alkane + alkene + aromatics, OVOCs, and isoprene, respectively.





ACPD
13, 1673–1716, 2013



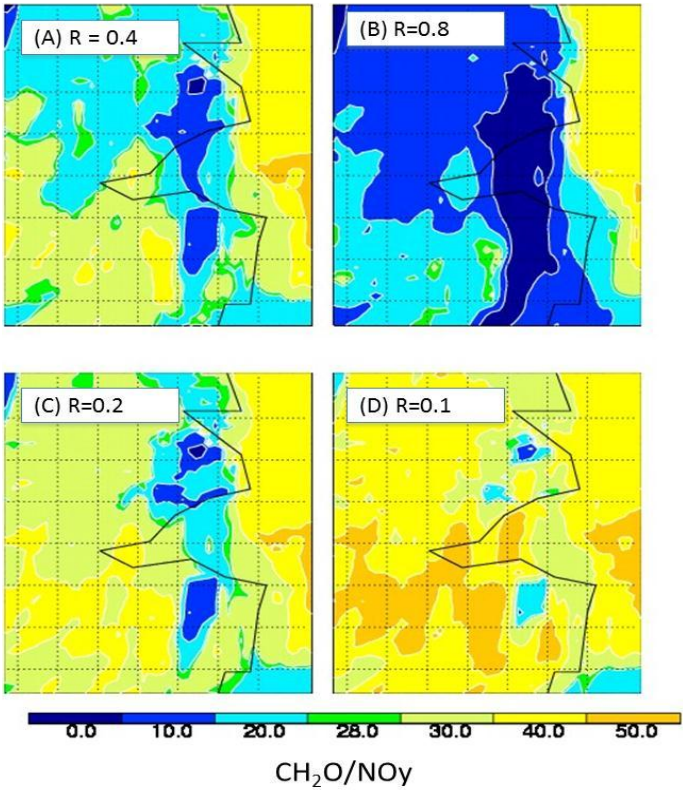


**Fig. 17.** The calculated ratio of $CH_2O/NO_y$ on 12 September in the Shanghai region, with different emission ratios of $NO_x$/VOCs in the model. The 4 panels represent different emission ratios, such as **(A)** with the ratio of 0.4, **(B)** with the ratio of 0.8, **(C)** with the ratio of 0.2, and **(D)** with the ratio of 0.1.





ACPD
13, 1673–1716, 2013